


Fatigue crack growth in micro specimens as a tool to measure crack–microstructure interactions

Patrick Grünewald  | Jonas Rauber | Michael Marx | Christian Motz | Florian Schaefer

Department of Materials Science and Methods, Saarland University, Campus D2 3, Saarbrücken, 66123, Germany

Correspondence

Patrick Grünewald, Department of Materials Science and Methods, Saarland University, Campus D2 3, 66123 Saarbrücken, Germany.
Email: p.grunewald@matsci.uni-sb.de

Funding information

Deutsche Forschungsgemeinschaft, Grant/Award Numbers: INST 256/340-1 FUGG, MO2672/1

Abstract

The process of short fatigue crack growth plays a significant role for the lifetime of materials in the high and very high cycle regimes. Fatigue crack growth is strongly influenced by interactions with microstructural obstacles, such as grain boundaries or phase boundaries, requiring a better understanding of these interactions to enhance the lifetime in these load regimes and improve lifetime calculations. Although it is possible to obtain crack growth rates from fatigue cracks in the lower micrometre range, further information like the exact position and type of the obstacle are mostly unavailable during the experiment. To overcome this issue, we propose a testing methodology of fatigue crack growth in micro specimens, which allows for an exact positioning of the crack relative to the obstacles and for monitoring the crack behaviour in a scanning electron microscope. The capabilities of this method are demonstrated for the interaction of fatigue cracks with grain boundaries.

KEYWORDS

compliance method, dislocation grain boundary interaction, micro bending beam, micro specimen, small fatigue cracks

1 | INTRODUCTION

The fatigue lifetime of cyclically loaded components can be attributed up to 90% to the initiation and growth of small fatigue cracks.¹ The behaviour of these cracks is largely influenced by their interaction with microstructural obstacles, like grain^{2–4} or phase⁵ boundaries. A systematic investigation of microstructurally short fatigue cracks is unfortunately not easily possible, as methods used to measure the crack behaviour in macroscopic specimens are mostly insensitive to fatigue cracks with sizes of only a few micrometres. Furthermore, to investigate the physics and mechanisms of short fatigue cracks

interacting with specific obstacles, it would be necessary to be able to precisely choose the location of crack initiation, how they grow and with which obstacle they will interact.

Multiple experiments to investigate the behaviour of short fatigue cracks with single obstacles are presented in the literature, some of which consider the three-dimensional nature of the problem. The methods used to monitor the crack behaviour range from using X-ray microtomography^{6,7} to using serial tomography by focused ion beam⁸ (FIB). Although this allows to correlate the crack growth behaviour to specific interactions, the problem remains that the crack front is geometrically not well defined and the crack will only show an

This is an open access article under the terms of the Creative Commons Attribution License, which permits use, distribution and reproduction in any medium, provided the original work is properly cited.

© 2020 The Authors. Fatigue & Fracture of Engineering Materials & Structures published by John Wiley & Sons Ltd

interaction with obstacles with a part of its crack front or even interact with multiple obstacles at once.

The modelling of short cracks and their microstructural interactions is also a relevant part of these investigations.^{9–12} Yet, due to the complexity of, for example, crack–grain boundary interactions, the models either have to generalize the grains and their boundaries to a few parameters like the grain size and misorientation angle¹² or reduce the three-dimensional system to a two or even one-dimensional model.⁹ Especially in the latter case, it is apparent that this assumption only holds true if the entire crack front interacts with the obstacle at once, which is hardly achievable with fatigue cracks in bulk specimens due to their arbitrary shape.

First steps to overcome these problems have been made in the past, where it has been shown to be possible to dictate the initiation site of fatigue cracks using notches cut with the FIB.¹³ However, the challenge remains to place specific obstacles in front of the fatigue cracks and also guarantee that the fatigue cracks interact with these obstacles with their entire crack front. Especially the latter has proven to be rather difficult, because the initiation site can be placed next to an obstacle, but the majority of the crack front will not grow in the direction of this obstacle in the case of a half-penny shaped crack in bulk specimens.¹⁴ Furthermore, not only the placement of the obstacles but also their type (e.g., grain or phase boundaries), shape (cubic, spherical and plate-like precipitates or curvature of a grain boundary) and alignment (e.g., the orientation of a grain boundary) decide whether this method is a suitable investigation tool. An almost perfectly straight grain boundary, for example, would be a suitable obstacle, whereas small, spherical precipitates can hardly be investigated by the presented method due to the curvature of their interface. If all of this is true for real cracks, it is important to showcase why the information of the simple case is necessary and helpful nevertheless.

A more advanced method is to initiate and grow fatigue cracks in micro bending beams using an in situ approach, as it has been done in previous experiments.¹⁵ Methods used to measure the crack length at the macro scale can be adapted to the micro scale experiments, because even short fatigue cracks make up a large portion of the overall specimen size. Methods that have proven to be suitable are measuring the crack length directly from micrographs in the scanning electron microscope (SEM) or calculating the crack length from the beam stiffness. It has been shown that both methods are in good agreement with each other. Yet, the measurement of the stiffness, and therefore the crack length, was only done at specific points during the fatigue procedure (e.g., every 500 cycles), resulting in a low number of data points. To be able to observe the interaction of the fatigue

cracks with obstacles, a high temporal resolution is necessary because the interactions occur and resolve mostly during just a few cycles. Furthermore, the fatigue cracks have been grown in Stage I so far and have shown a strong interaction with the neutral axis of the bending beams. This interaction might be problematic as it may overlap with potential crack–obstacle interactions.

The aim of the present work is to show that it is indeed possible to increase the temporal resolution up to the point that the crack length can be calculated for every cycle by further improving the experimental set-up. Besides this, Stage II fatigue cracks show a negligible interaction with the neutral axis, contrary to their Stage I counterpart, due to their multislip nature and lessened dependency on single dislocation pile-ups. The applicability of this technique was tested by incorporating grain boundaries as obstacles inside the micro bending beams. We observed that fatigue cracks interacting with the same type of grain boundary showed similar deceleration, whereas when compared with cracks interacting with other types, the differences were evident.

2 | METHODOLOGY AND EXPERIMENTAL SET-UP

In the following, methodology and experimental set-up will be described. The set-up is described in more detail in preliminary work,¹⁵ wherefore it will be summarized quickly and only the changes and enhancements will be described extensively.

2.1 | Material selection

The nickelbase-superalloy CMSX-4 we use in this work is a suitable model material for our purposes as it has a high strength, cubic face-centred lattice structure (relevant for the investigation of dislocation interactions) and a microstructure that favours single-slip behaviour. Especially the latter is of particular interest to grow cracks solely in Stage I to set up specific dislocation configurations.^{8,13,14} Responsible for this single-slip behaviour are the γ' precipitates, whose coherent phase boundaries did not show any noticeable effect on the crack growth behaviour so far and will therefore not negatively affect our experiments. The high strength helps with being able to apply enough driving force on these short cracks without plastic deforming the rest of the bending beam. This aspect will be discussed in more detail later on, as it is relevant for the transferability of our technique to other materials. Furthermore, this material has a high elastic anisotropy, which can be beneficial if the influence of misfit stresses

at grain boundaries is to be investigated but complicates the evaluation otherwise because the elastic stiffness tensor has to be used instead of scalar parameters.

2.2 | Specimen preparation

The micro bending beams, as well as the manipulators used for the fatigue experiments, are cut using the FIB milling technique, as extensively described in existing literature. A FEI HELIOS Nanolab 600 was used for milling the specimens and the manipulators with an acceleration voltage of 30 kV and beam currents starting from 20 nA down to 1 nA for most of the milling steps and a beam current of 50 pA for the notches in the bending beams. The specimens have an aspect ratio of 1:4, a square cross-section and a thickness of 15 μm , as schematically drawn in Figure 1. The notches have a depth of about 2 μm with slight deviations between the specimens due to differences in the exact cutting time in the FIB.

The comparably larger size of the specimens has two reasons. First, micro specimens are prone to showing plasticity size effects, especially under bending conditions. These size effects, like strain gradient plasticity, are mostly dominant in the lower micrometre range,^{16,17} wherefore the effects start to vanish for the beam size used in our experiments. Second, because we can gather more data for the crack growth curves the longer the fatigue cracks grow, larger beam sizes provide us with more space for these cracks to grow. This is especially relevant when measuring crack–obstacle interactions, as the crack can then freely grow for some time before sensing the obstacle, which would be required to measure the deceleration.

For the case study of the crack–grain boundary interactions, the micro specimens have been cut to incorporate the desired grain boundaries. Due to the presence of a potential neutral axis interaction, the grain boundaries were not placed in the middle of the beams to prevent a possible overlap of interactions. Yet, due to a decreasing ligament, the neutral axis will be displaced during crack

growth, so that a potential overlap of these interactions cannot be eliminated completely. The best set-up would be to place the grain boundaries closer to the notch, so that the grain boundary interaction happens before a potential neutral axis interaction, but because this would limit the space for the fatigue cracks too much, the grain boundaries were placed on the opposite site of the beams instead. When testing larger specimens, for example, micro specimens cut using a plasma FIB, it would be possible to position the grain boundary between notch and neutral axis, thus eliminating the overlap of these interactions. As will be demonstrated later in Section 2.5, this interaction with the neutral axis vanishes when Stage II cracks are used instead of Stage I cracks, wherefore the potential overlap of a neutral axis interaction and grain boundary interaction is also negated.

Two types of manipulators had to be cut for the fatigue loading procedures, a gripper used for the crack initiation and a wedge used for the monitoring phase. The gripper can load the micro bending beams in two directions to provide a higher driving force for crack initiation, whereas the wedge can only apply load in one direction but allows for a more stable mode of operation (will be explained in the next section in more detail). The manipulators are made of tungsten carbide to provide as much stiffness as possible to reduce an influence on the measured stiffness used to calculate the crack length during the experiments. Micrographs of both types of manipulators are shown in Figure 2.

2.3 | Loading procedures

The experiments have been conducted in situ in a TESCAN VEGA SEM using the nanoindentation module Asmec/Zwick Roell UNAT 2 to load the specimens. The tungsten carbide manipulators were installed in place of the normal indentation tips. The nanoindentation module is intrinsically displacement controlled but still allows two modes of operation: displacement and force control.

In the past, displacement control has been proven to be suitable to initiate and grow fatigue cracks in micro bending beams, but the system is susceptible to thermal drift, resulting in the need to reposition the manipulator every few hundred cycles. Because it is nearly impossible to place the manipulator at the exact same position every time, the applied load is very unstable during the fatigue loading. The applied load maximum in the crack opening direction is shown in Figure 3 over multiple thousand cycles during one of the experiments. It is obvious that this instability would negatively affect the loading state and the evaluation of the stiffness during the experiment, and hence the crack length and crack growth curves.

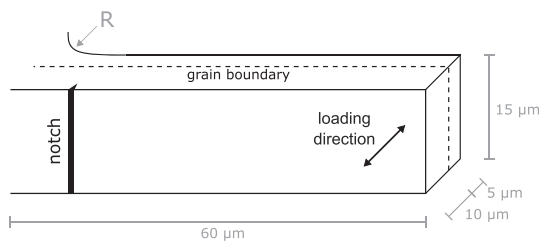


FIGURE 1 Schematic of the micro bending beams cut by FIB. In the case of the bicrystalline specimens, a grain boundary was placed at the marked position

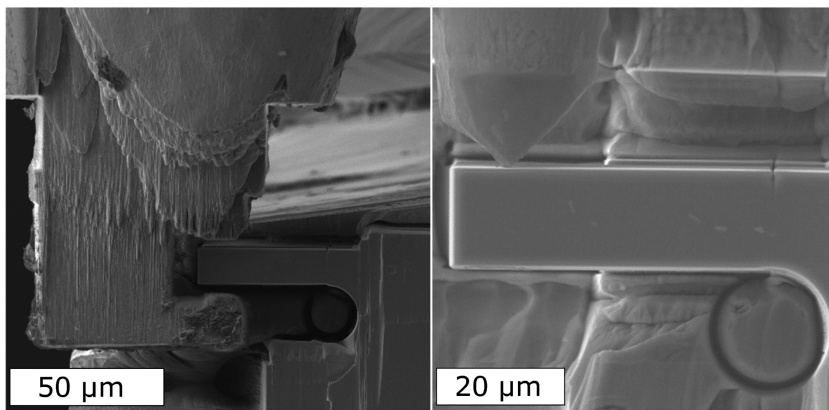


FIGURE 2 Scanning electron microscope micrographs in secondary electron contrast of the gripper (left) and the wedge (right) used to load the micro bending beams

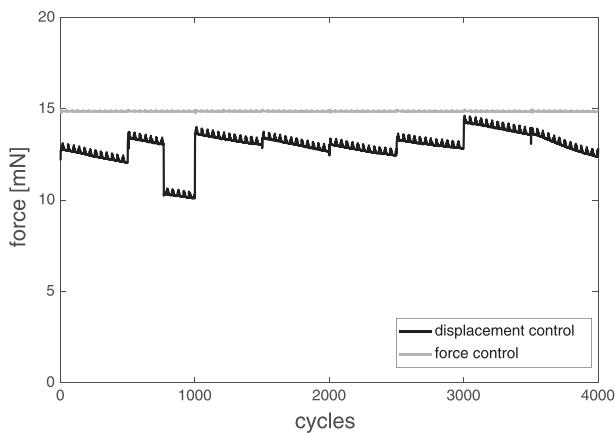


FIGURE 3 Applied load during cyclic loading in displacement and force control respectively. Gripper and wedge have been readjusted every 500 cycles

A more stable load level can be achieved by using force-controlled loading, as also shown in Figure 3. But because the nanoindentation module requires the tip to do a surface approach prior to executing the loading procedure, the gripper cannot be used for load-controlled crack growth. Hence, the wedge is used to load the beams under force control.

Using the gripper has the advantage of being able to apply negative forces, whereas the wedge can only apply positive forces. Because the positive stress ratios have proven to be insufficient to initiate fatigue cracks in micro specimens of highly ductile materials and the gripper can only be used with unstable load levels, a mixture of both techniques have been used during the fatigue procedure, where the gripper is used under displacement control to initiate and grow a small fatigue precrack and the wedge is used under force control afterwards to grow the fatigue cracks under constant load amplitude and monitor the crack growth rate.

To force the crack initiation to occur at the notch and not at the opposite side of the beam, we used a

displacement ratio resembling a stress ratio of approximately -0.8 for the gripper. For the wedge, we used a stress ratio of 0.1 to maximize the driving force without losing contact during loading. A schematic summary of the overall fatigue procedure is given in Figure 4.

2.4 | Determination of crack growth curves

In the following, we will describe the general methodology of calculating the crack growth rate from measured and co-simulated data and also include example data from one of the grain boundary experiments to visualize the steps.

As mentioned before, the experimental set-up allows for two methods of acquiring the crack length: measured from SEM micrographs and calculated from the beam stiffness. The first method is dependent on the lateral resolution of the SEM, whereas the second method depends on the resolution of the force and displacement signals. Due to the in situ nanoindentation module in the SEM chamber, the working distance is larger than 25 mm, which in combination with a tungsten filament SEM and a high beam current (needed to get enough contrast with a low signal to noise ratio) results in an insufficient resolution of the SEM micrographs. Furthermore, even though both methods lie in a good agreement with each other,¹⁵ an evaluation based on the stiffness of the bending beams is more desirable because crack fronts can never be expected to be perfectly straight and thereby also not completely visible on the surface.

The resolution of the stiffness on the other hand has proven to be sufficient for our purpose. Taking a micro beam without a notch or crack, we can measure the fluctuation of the calculated stiffness by loading the beam for a few hundred cycles with different loading and sample rates, as shown in Figure 5. The accuracy of the stiffness measurement seems to improve with increasing loading

FIGURE 4 Applied load during our experiments, showing the transition from displacement control to load control. The load is increased carefully after the transition to not accidentally deform the specimens plastically

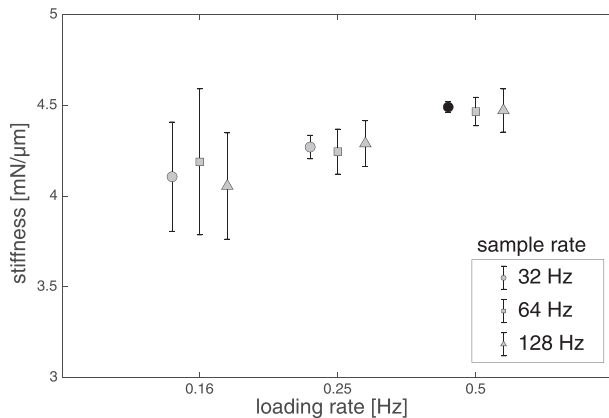
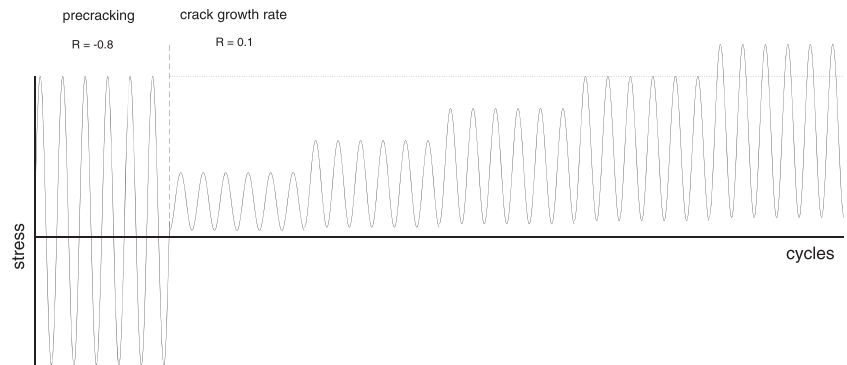


FIGURE 5 Mean value and standard deviation of the measured stiffness for different choices of loading and sample rate. The parameters used during the experiments are marked in black

rate, which can be attributed to the fact that the control errors of the nanoindentation module, which was originally not developed with cyclic loading of micro specimens in mind, are more pronounced at lower loading rates. The data sample rate on the other hand shows almost no influence on the measured stiffness itself but on its fluctuation, which results from the stored data values being intrinsically smoothed at lower sample rates.

A dependence of the mean value of the measured stiffness on the loading rate can be observed, but because we work with the stiffness being normalized regarding the initial stiffness, this will not influence the calculated crack length as the loading rate was kept constant during the tests.

From the stiffness, the crack length a can now be calculated for each load cycle N and with that the crack growth rate da/dN . Calculation of the driving force is combined with the calculation of the geometry factor from the finite element simulations. Because our specimens are loaded in the elastic regime for the crack growth curves, the cyclic stress intensity factor ΔK was

chosen as the parameter describing the driving force. The driving force ΔK was not directly calculated from the finite element simulations, instead we calculated the elastic J -integral due to higher numerical accuracy and accessibility.¹⁸ The elastic-plastic cyclic J -integral has some shortcomings as a parameter for the driving force, especially the fact that the elastic-plastic behaviour is approximated by nonlinear elasticity, which is invalidated when unloading events occur. Yet, because our specimens are loaded in the elastic regime, and we only calculate the elastic J -integral from our finite element simulations, a conversion from this elastic J to ΔK is valid.

For each specimen, a separate finite element simulation was conducted to take beam size, position of the grain boundary, crystallographic orientation and position of the tip on the beam into consideration. The only remaining variable is the applied force, which can be used to normalize the J -integral. Because the J -integral is proportional to the stress intensity factor squared, which is in turn proportional to the force, the J -integral is normalized by the force squared.

The full procedure is schematically summarized in Figure 6 and will now be explained step by step:

1. Measure force F and displacement signals u and calculate the stiffness S from these data for each cycle N_i .
2. Run finite element (FEM) simulations to get the dependency of the stiffness on the crack length a , also taking crystal orientations of both grains, elastic stiffness tensor S_{ijkl} and position of the grain boundaries into account for each individual specimen (2a). Use the same simulations to also calculate a geometry factor in form of the J -integral normalized regarding the square of the applied force over the crack length (2b). A description of the simulation parameters and the model is given in a previous publication.¹⁵
3. Use the simulated and measured stiffness values to calculate the crack length for each cycle. At this point, the crack length needs to be measured once from a micrograph to transform the measured stiffness values

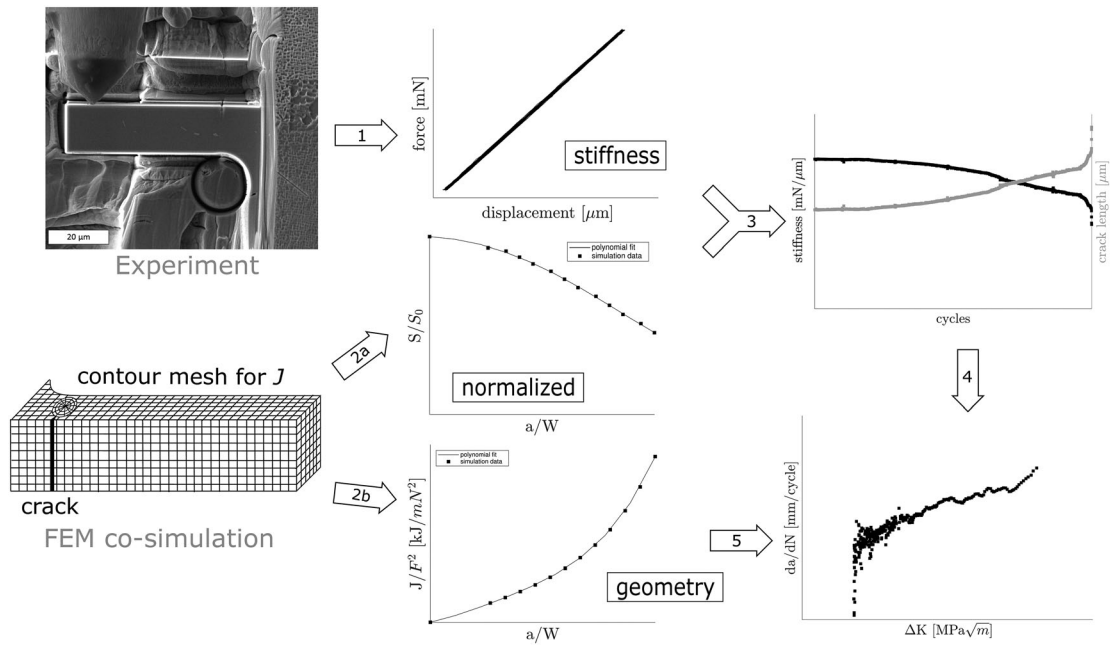


FIGURE 6 Procedure to determine the crack growth curves from experimental and simulated data, divided into five individual steps

S into normalized ones S/S_0 to account for small variations of the geometry and the machine compliance.

- Fit a moving second-order polynomial with parameters P_n and calculate the crack growth rate $(da/dN)_i$ as follows:

$$a_{\text{fit},i} = P_{2,i} N_i^2 + P_{1,i} N_i + P_{0,i}, \quad (1)$$

$$\left(\frac{da}{dN}\right)_i \approx \left(\frac{da_{\text{fit}}}{dN}\right)_i = 2P_{2,i} N_i + P_{1,i}. \quad (2)$$

Vary the span length to find a parameter set that reduces the scatter without introducing artefacts to the curves.

- Use the normalized J -integral J_i^{norm} from the FEM simulations as a geometry factor in addition to the amplitude of the applied force ΔF_i per cycle to calculate the driving force ΔK_i as follows:

$$\Delta J_i = \Delta F_i^2 J_i^{\text{norm}}, \quad (3)$$

With ν being the Poisson ratio and E the Young modulus in the direction of the beam axis, which have been calculated by measuring the crystal orientation with electron backscatter diffraction (EBSD) and using the elastic stiffness tensor¹⁹ (measured by ultrasound measurements).

The large amount of data points acquired this way leaves room to average over multiple data points

afterwards. The resulting crack growth curves depend strongly on the choice of parameters for the polynomial fit of the crack length as well as the number of data points that get averaged finally, as is demonstrated in Figure 7. It is therefore crucial to run a parameter study on each and every data set to evaluate with which parameters the artefacts and too much scatter get eliminated while actual features still remain.

When the parameters are chosen too loose, the curves are closest to the real data, but the large amount of scatter hinders a further evaluation of the curves. On the other hand, if the parameters are chosen too tight, the data gets smoothed too much, resulting in a too low number of data points in the case of strong averaging and the characteristic round shapes due to a convolution of a large span size second-order polynomial with the real data. A curve after postprocessing with a suitable parameter set is shown in Figure 7 (right), which was then taken for further analysis in this form.

2.5 | Stage I versus Stage II crack growth

Stage I cracks have been the method of choice in previous experiments, due to the fact that the dislocations emitted from the crack tip are from a single and well-known slip system and, depending on the material, Stage I fatigue cracks can grow for up to multiple micrometers and are the main actors in the crack–obstacle interactions in these cases. On the other hand, Stage II cracks are the normal case for long cracks in macroscopic fatigue of

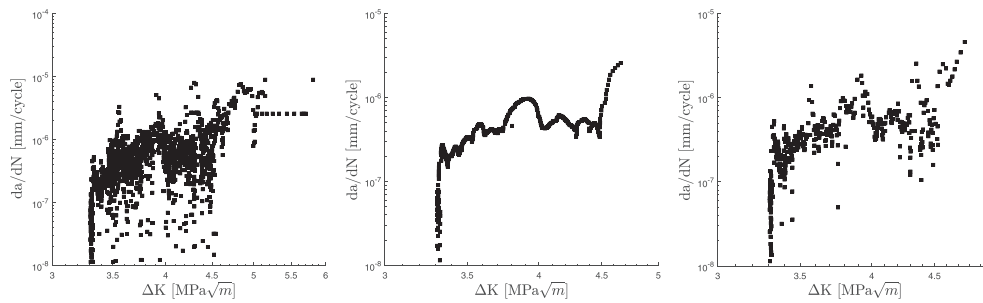


FIGURE 7 Exemplary crack growth curves for an experiment where interactions of a crack with an obstacle occur. Postprocessing was done using different parameter sets: (left) loose, resulting in too much scatter (centre) tight, resulting in artefacts from postprocessing (right) suitable for our experiments

most industrial alloys. Because the notches in macroscopic bulk specimens can be cut longer than the ones in micro specimens, comparable driving forces can be achieved with lower stresses. This means that any slip system is a suitable candidate as long as it has the highest Schmid factor in the grain, independent of the direction of the Burgers vector. In micro specimens on the other hand, the orientation needs to be chosen so that one of the slip systems has a Schmid factor of 0.5 and a Burgers vector pointing in the crack growth direction. Because the crystallographic orientation of the bending beams then dictates the orientation of the notch or crack plane, there would only be one geometrical orientation of the bending beams suitable for Stage I fatigue crack growth. If specific grain boundaries are to be placed along the axis of the bending beams, for example, the crystallographic orientation cannot be chosen freely anymore, which results in the cracks growing in Stage II inevitably.

Furthermore, as previous experiments have shown,¹⁵ although it is indeed possible to grow cracks purely in Stage I in micro bending beams, their slip system needs to be orientated under 45° to the beam axis. This requires elaborated sample preparation, which will still not guarantee the growth of Stage I cracks as can be seen in Figure 8.

Another problem of Stage I fatigue cracks in micro bending beams is their neutral axis interaction that alters their crack growth rate. In comparison, in the absence of a grain boundary, the crack growth rate monitored for a Stage II crack in Figure 9 shows no noticeable deceleration or interaction, even for a large growth distance. This unhindered crack growth of the Stage II cracks can be attributed to their multislip nature and, as a result, their lower dependence on a single dislocation pile-up at the neutral axis. Whereas a Stage I crack grows on a single slip plane and is hence slowed down by a dislocation pile-up, Stage II cracks can switch their growth direction and hence circumvent the influence of the dislocation pile-ups. For a measurement of interactions between

cracks and grain boundaries, Stage II cracks have proven to be the more suitable tool and were therefore used for the following experiments.

3 | APPLICATION EXAMPLE: GRAIN BOUNDARIES

The following chapter demonstrates the technique for two different grain boundary set-ups. More examples of this method in use are presented in previous work.²⁰

3.1 | High-angle grain boundary

An SEM micrograph and the corresponding crack growth rate for this grain boundary can be seen in Figure 10A,B. It is clearly visible from the crack growth rate that the crack has undergone some sort of interaction with the grain boundary. The force-controlled propagation of the crack can be separated into three phases, as indicated by the labelled arrows. At first, the crack has grown out of the notch inclined followed by a deceleration of the crack

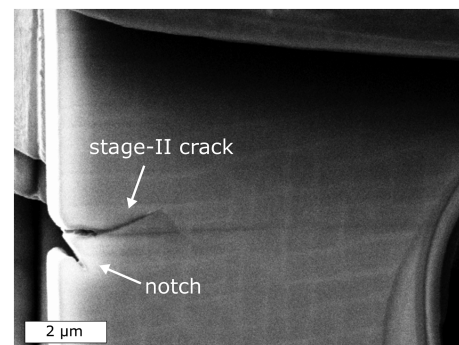


FIGURE 8 Micro bending beam with a crystallographic orientation suited for Stage I crack growth. Yet, in this case, the crack still grew in Stage II

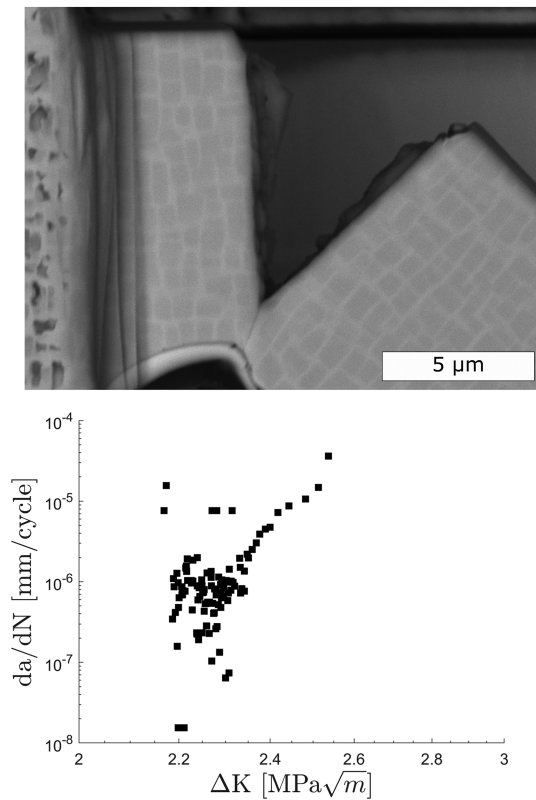


FIGURE 9 Scanning electron microscope micrograph in backscatter electron contrast of a Stage II crack grown through most of the bending beam with the respective crack growth rate. The growth rate shows a strong fluctuation in the beginning part, but stabilizes after reaching some momentum. Due to a high crack growth rate, the number of available data points near the end is very scarce

growth before changing its direction (transition from I to II). The crack has started to accelerate again after its change in the growth direction, just to slow down again when sensing the grain boundary (II). The last phase is the longest in terms of crack propagation but the shortest in terms of cycles (III). In just a few cycles, the crack has rapidly grown over the grain boundary. This resulted in a

rapid plastic collapse of the micro bending beam, due to applying a constant load amplitude during force-controlled fatigue while the cross-sectional area decreases as a result of the continuous accelerated crack growth. This abrupt change in crack growth rate and the passing of the grain boundary suggests that the crack was slowed down by the grain boundary interaction up to the point where it was able to overcome this blockade, similar to the experiments conducted on macroscopic specimens in the past.¹⁴

To determine the strength of the blockade, we have used a power-law fit for the part of the crack growth curve before any interaction with the grain boundary, comparable with the Paris–Erdogan equation for macroscopically long cracks. Afterwards, the point of the slowest crack growth rate before the crack has rapidly grown across the grain boundary was determined, but due to high scatter of the data points, we have not used the single lowest point but rather the crack growth rate where most data points coincided. This value was then compared with the crack growth rate this crack would have had if it would not have been blocked by a grain boundary, which was calculated by using the power-law fit and the value of ΔK at the deceleration point. This has given us a relative deceleration as a quantity to define the strength of the grain boundary resistance. This procedure was calculated by Equation 5 and is schematically shown in Figure 10C.

$$\Delta v_{\text{rel}} = \frac{da/dN}{C(\Delta K^{m_{\text{short}}})}. \quad (4)$$

The crack growth curve observed in a second beam, tested on the same type of grain boundary, is plotted together with the first beam in Figure 11. The gathered values of the micro specimens with the high-angle grain boundary are shown in Table 1, together with the values of the small-angle grain boundary specimen. Both curves are in good agreement regarding their values of ΔK , da/dN

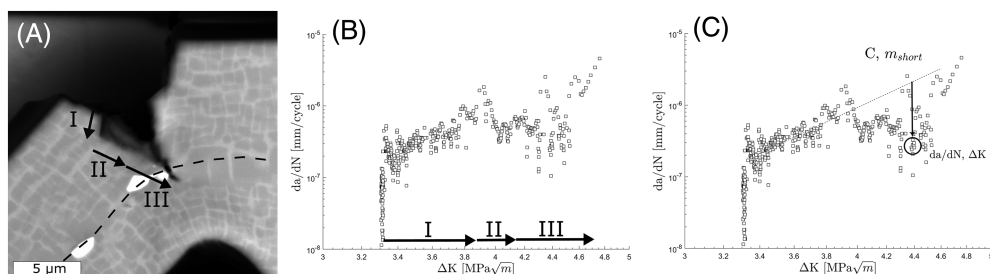


FIGURE 10 (A) Scanning electron microscope micrograph in BSE contrast of crack interacting with a grain boundary (dashed line). The three phases of crack growth are marked with arrows. (B) Crack growth rate, also including the arrows marking the three phases. (C) Evaluation of the relative deceleration from the gathered crack growth curve, marked with an arrow

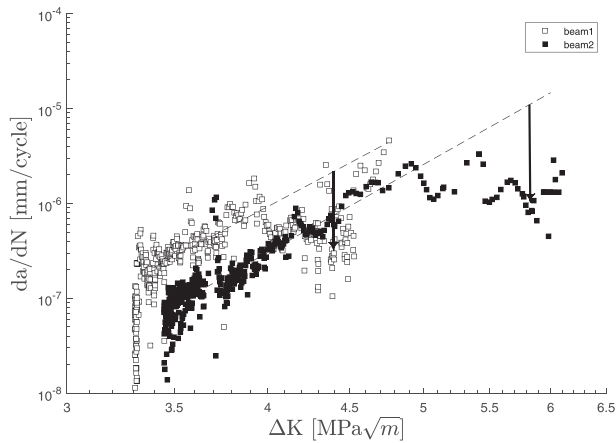


FIGURE 11 Crack growth rate for two micro bending beams tested at the same grain boundary. The relative deceleration is marked with an arrow for each of the curves

dN and the relative deceleration at the grain boundary. Especially the latter, which is the quantity of interest for our investigations, is indicative of an acceptable reproducibility, although the experimental set-up is complex and there are plenty of influencing factors.

3.2 | Small-angle grain boundary

To check what is measurable in addition to a principal influence of a crack–grain boundary interaction on the crack propagation, we have considered the relative decelerations for a second type of grain boundary, namely, a small-angle grain boundary. The corresponding crack growth rate for this configuration is given in Figure 12.

Despite the fact that the crack showed no deflection when approaching the grain boundary, the influence from the grain boundary can be seen in the crack growth rate. An abrupt acceleration of the crack (indicated by the change of slope) can be distinguished, but the deceleration cannot be determined as clearly. The data points marked by the arrow in Figure 12 could show the deceleration but could also just be due to scatter. The relative deceleration deduced from these data is hence given with

parenthesis in Table 1 to factor in its uncertainty. These data indicate that the crack may also slow down when approaching a small-angle grain boundary, yet the slow-down is not as pronounced as in the case of the large-angle grain boundary or even completely absent. The change of slope on the other hand is a clear indicator that the crack growth behaviour has changed after overcoming the grain boundary interaction.

4 | EVALUATION OF THIS TECHNIQUE

In the following, we will discuss the methodology of this novel technique, especially which data can be extracted from these experiments or how reproducible it is and whether it can be applied to other materials or obstacles as well. The information gathered from the grain boundary experiments will also be included in the discussion, as they deliver valuable insight on the applicability of the technique.

4.1 | Obtainable information

The data that can be gathered from this technique can be divided into two parts: information about the crack growth itself and information about the obstacle.

Because the first one is decoupled from the obstacle interaction, we can use the crack growth curves from the single crystals and compare them with the grain boundary specimens. All bicrystalline specimens have a slope m_{short} in the range of 9, whereas there were single crystalline specimens²⁰ with an m_{short} of over 12. Taking a look at the crystal orientations, the grains where the cracks of the bicrystals initiated had a similar crystallographic orientation ($\theta \sim 11^\circ$) with four slip systems having high and similar Schmid factors ($\langle 110 \rangle$ direction in beam axis), whereas the crystal orientation with the high slope had eight slip systems with a similar Schmid factor of the same magnitude as for the bicrystalline case ($\langle 100 \rangle$ direction in beam axis). This indicates that we can also observe an influence of the slip behaviour on the crack

TABLE 1 Parameters of the investigated grain boundaries (misorientation angle θ) and the crack growth (slope m_{short} , fit parameter C , starting value ΔK_{st} , stress intensity factor at the point of highest deceleration ΔK and relative deceleration Δv_{rel})

Bending beam	θ ($^\circ$)	m_{short}	C	ΔK_{st} (MPa $\sqrt{\text{m}}$)	ΔK (MPa $\sqrt{\text{m}}$)	Δv_{rel} (%)
1	29.7	9.01	3.48E–12	3.32	4.40	82.23
2		9.56	5.34E–13	3.46	5.79	92.05
3	9.0	9.76	6.95E–13	3.61	4.57	(31.54)

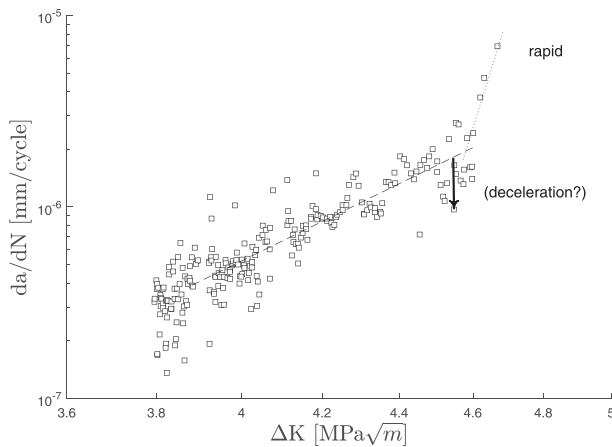


FIGURE 12 Crack growth curve for the small-angle grain boundary. The deceleration point is not as pronounced as in the large-angle grain boundary, but the switch to the rapid growth regime is distinguishable. The relative deceleration is again marked with an arrow

growth rate, resulting in a higher slope the higher the number of active slip systems.

In regards to the obstacle interactions, the experiments have shown that we can not only observe a deceleration due to the interaction but can also see an influence of the type of interaction on the strength of the deceleration. Still, further parameter studies are required to make a statement on the influence of the grain boundary type on the crack deceleration. Although our results seem to underline the assumptions made in De Los Rios et al.¹² so far (fatigue crack growth of short cracks hindered by obstacles, followed by acceleration, deceleration at the next obstacle a.s.o.), it is unclear whether this holds true for all grain boundaries or if it was just the case in the specimens investigated in this work, especially because not only the misorientation but also the overall structure of the grain boundary changed (disordered random large-angle grain boundary versus ordered small-angle grain boundary). To describe the crack–grain boundary interaction fully, a large parameter study would be necessary. Nevertheless, our results indicate that this technique serves as a suitable tool to conduct this parameter study.

Another advantage of this technique is that not only the crack growth curves are obtainable but also visual information of the crack behaviour. This is evident considering the first tested beam. Although the crack growth curve showed two deceleration events, only one of them corresponds to a grain boundary interaction. With the help of the SEM, it was possible to correlate which of these events correspond to which phase in the crack growth curves.

4.2 | Reproducibility

The reproducibility can also be evaluated based on the crack growth behaviour itself and the strength of the interaction. As mentioned before, for similar crystal orientations, the gathered crack growth curves are in a good agreement with each other, especially regarding the slope m_{short} . The starting value of the stress intensity factor, ΔK_{st} , which should also not be mistaken for the threshold value of long fatigue crack growth, does not contain any information because it depends on the length of the crack when switching from displacement control to load control and can hence not be used to evaluate the reproducibility in terms of the crack growth behaviour. Yet, because the load was increased stepwise after switching from displacement to load control and because the cracks had comparable lengths at this stage, the values of ΔK at which the cracks continued growing should not differ too much, as can be seen in Figure 11 for example.

The relative deceleration, which would be the quantity of interest when investigating crack–obstacle interactions, does show a slight difference between tests conducted on the same grain boundary type. Yet, especially given the fragility of the experimental set-up (which is prevalent for experiments on micro specimens), this small deviation can be considered to be in an acceptable range. This results in a good reproducibility of the technique, given the currently available data, as it is important for experiments where the financial and temporal expenditure requires that, in the best case, every specimen delivers reliable results and where statistical data is hardly available.

4.3 | Comparison with macroscopic crack growth rate

Because it is well known that micro specimens can show mechanical behaviour that deviates strongly from the macroscopic behaviour,^{16,21} it is mandatory to compare the microscopic mechanical behaviour with its macroscopic counterpart. Short fatigue crack growth resembles an exception to this rule, as the overall topic of interest is the behaviour of short fatigue cracks in macro specimens where the crack length is in the same range as our fatigue cracks. Yet, a comparison of our fatigue crack growth behaviour with that of longer fatigue cracks in the same material could deliver insights on the behaviour of short fatigue cracks in general. For this comparison, fatigue cracks have been monitored on three different length scales: lower micrometre range, upper micrometre range and lower millimetre range. Crack growth curves for all length scales are plotted together in Figure 13, where it can be seen that with increasing size of the fatigue crack,

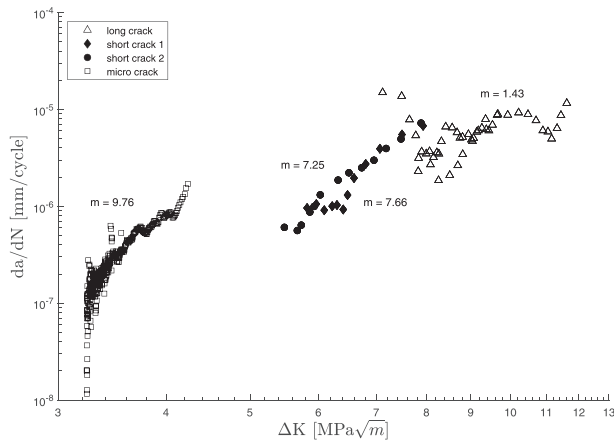


FIGURE 13 Crack growth curves of the same material for three different length scales. The data were gathered by testing: micro specimens, tensile specimen with FIB notch and tensile specimen with long fatigue crack

the applied driving force increases while the slope decreases. Furthermore, it can be seen that the short fatigue cracks presented in this work reach the same values of da/dN for lower values of ΔK . This shows us that short fatigue cracks grow rapidly when compared with macroscopically long fatigue cracks, only restrained by their microstructure interactions, as described in the aforementioned literature.^{4,12} This further underlines the necessity to investigate and understand the interaction of these short cracks with microstructural obstacles and their impact on the overall lifetime. Not only do the cracks grow faster but also at values of ΔK that can be lower than the threshold ΔK_{th} of long fatigue cracks.

Another distinctive difference to macroscopic crack growth lies in the influence of crack closure. Because the experiments are conducted under vacuum conditions in the SEM, oxide-induced crack closure is negligible compared with fatigue crack growth in air. Plasticity-induced and roughness-induced crack closure on the other hand do not directly depend on the testing atmosphere and need to be discussed as well.

Given the same driving force, and hence a similar crack opening displacement, the relative opening of the crack compared with the specimen size is larger at the micro scale. An example of this can be seen in Figure 9, where the specimen was loaded in the elastic regime during fatigue crack growth but the specimen shows a crack opening of around half the beam thickness. Due to this large crack opening, and the positive stress ratios, roughness-induced crack closure is negligible for these specimens. Yet, this explanation is not as straightforward when the crack deflected during growth, as seen in Figure 10, or where the crack path is faceted and roughness-induced crack closure could therefore still occur in these cases.

In contrast to oxide-induced and roughness-induced crack closure, plasticity-induced crack closure cannot be easily neglected and may even play a greater role. As plasticity-induced crack closure plays a more significant role in plain-stress condition compared with plain-strain condition,²² and crack growth is only dominated by plain strain when large specimens are tested (e.g., on the macroscopic scale), plasticity-induced crack closure is more pronounced in our plain-stress-dominated micro specimens.

4.4 | Transferability to other materials and obstacles

So far, the experiments have only been conducted on our model material. Because this technique is presented as a possible tool to investigate the crack–obstacle interaction for different materials and obstacles, the question arises whether this method is transferable. The type of obstacle itself is not of greater importance to the transferability, as the fact whether the cracks interact with these obstacles is the matter of investigation. The shape of the obstacle on the other hand plays a significant role. The strength of this method compared with experiments in the existing literature stems from the fact that the crack interacts with the obstacle with its whole crack front at once, resulting in a measurement of this interaction alone without outer disturbances. If the shape of the investigated obstacle is too inhomogeneous, this assumption does not hold true anymore and the strength of this technique vanishes, for example, for precipitates with complex shapes or small sizes.

Whether this method is suitable for a given matrix material depends on a few factors like, for example, the strength of the material. Because the driving force for crack growth, namely, the stress intensity factor or the J -integral, are not only dependent on the applied load but also the crack length, higher loads are necessary in the micro specimens compared with macroscopic specimens to reach the same driving force. If the material requires too much driving force to initiate and grow these fatigue cracks while simultaneously having a low strength, the challenge lies in being able to apply enough driving force without plastically deforming the specimen beforehand. This technique is therefore less applicable to pure metals, whereas materials that exhibit hardening on a length scale smaller than the obstacle of interest (e.g., solid-solution hardening or nanoscale precipitates) are suitable candidates for this technique.

Besides the transferability of the technique, the transferability of the results must also be considered. If the mechanisms investigated by this technique are

independent of material specific quantities (like crack-grain boundary interactions), the experiments could be conducted on model materials that offer the requirements like high strength.

4.5 | Role of size effects

Plasticity size effects in micro bending beams are mainly attributed to two effects, which may occur alone or together. The first one is the formation of a dislocation pile-up at the neutral axis of the beam, whose backstress then alters the activation stresses of adjacent dislocation sources.¹⁶ The second explanation is the strain gradient plasticity, which is based on the fact that decreasing the beam size leads to an increase in the strain gradients when the applied deformation is to be the same. Due to a decreased distance between geometrically necessary dislocations in these steeper gradients, strain gradient plasticity increases the flow stress of the bending beams¹⁷ or the gradients in front of crack tips.²³

As mentioned in Section 2.2, we chose a beam thickness large enough so that these size effects should be negligible. Yet, the growing fatigue crack will decrease the size of the ligament and by that increase the gradient in front of the crack tip. The elastic strain gradient is partly considered in our approach due to calculating the geometry factor from finite element simulations. The driving force was calculated for multiple crack lengths, and because we made a separate simulation for each of these crack lengths, the effect of the elastic strain gradient in front of the crack tip is included. Yet, because our finite element simulations only use elastic material behaviour, they do not necessarily reflect the true effect when plasticity comes into play. Therefore, we can unfortunately neither ignore the role of the strain gradient plasticity nor can we measure its influence given our experimental set-up.

4.6 | Improvements and outlook

Even though we were able to use this technique in its current state for first experiments, there are possibilities to improve this set-up further. Especially the reproducibility could and should be further improved, for example, by implementing a set-up that can conduct the crack growth experiments with a constant ΔK . This would require an automatic evaluation of the current crack length, for example, from the stiffness, and a subsequent adjustment of the applied force. In the current state, the testing module used for these experiments can only apply a constant force for any given loading period and changing the force can only be underdone by stopping the

loading and restarting it again with a new force level. When applying a constant ΔK , the crack growth rate should stay constant for unhindered crack growth, wherefore changes in the crack growth rate due to interactions should be discoverable more easily.

Furthermore, a change of specimen geometry could also improve this technique, for example, by investigating micro tensile specimens instead of bending beams. The homogeneous, uniaxial stress and the absence of a neutral axis would greatly reduce factors influencing the crack growth and crack-microstructure interactions. On the other hand, micro tensile specimens are significantly harder to manufacture and test correctly, especially if cyclic loading is to be applied.

5 | CONCLUSION

We were able to show that it is possible to initiate fatigue cracks in micro specimens in a reproducible manner. Furthermore, the crack growth rate can be monitored with both a good temporal as well as spatial resolution. Single deceleration events can be measured, like crack deflection or grain boundary interactions, and also be correlated to the crack behaviour by using an in situ set-up in the SEM. Differences in the strength of the deceleration can be measured for different types of obstacles, which allows this technique to be used to measure single crack-obstacle interactions. Experimental difficulties and suggestions on how to overcome them are presented in detail to allow this technique to be reproduced and adapted by other research groups.

ACKNOWLEDGEMENTS

The authors are indebted to our colleague Lena Eisenhut for her preliminary work and Christoph Pauly (Materials Engineering Center Saarland) for his assistance during the experimental work. We thank Jan Grodzki (University of Erlangen-Nuernberg) for manufacturing the sample material. Open access funding enabled and organized by Projekt DEAL.

CONFLICT OF INTEREST

The authors fully disclose any conflict of interest for the presented work.

FUNDING INFORMATION

This work was supported by Deutsche Forschungsgemeinschaft (MO2672/1). The SEM used for the presented experiments was financed by the DFG under grant number INST 256/340-1 FUGG. We gratefully acknowledge the financial support by the Deutsche Forschungsgemeinschaft.

NOMENCLATURE

a	crack length
a_{fit}	crack length from polynomial fit
C	fit parameter for Paris–Erdogan like power law
da/dN	crack growth rate
E	Young's modulus
F	force
ΔF	force amplitude during cyclic loading
J	elastic J-integral
J^{norm}	normalized elastic J-integral from FEM simulations
ΔJ	cyclic elastic J-integral
K	stress intensity factor
ΔK	cyclic stress intensity factor
ΔK_{st}	cyclic stress intensity factor at the beginning of load-controlled testing
m_{short}	exponent of power-law fit, slope of crack growth rate in log–log scale
N	number of cycles
P_n	fit parameter for polynomial fit
R	stress ratio
S	beam stiffness
S_0	beam stiffness in absence of notches or cracks
S_{ijkl}	elastic stiffness tensor
u	displacement
Δv_{rel}	relative deceleration
θ	misorientation angle

ORCID

Patrick Grünewald  <https://orcid.org/0000-0002-7099-0594>

REFERENCES

- Krupp U. Mikrostrukturelle Aspekte der Rissinitiierung und -ausbreitung in metallischen Werkstoffen. Habilitation thesis: Universität Siegen. 2004
- Chang R, Morris WL, Buck O. Fatigue crack nucleation at intermetallic particles in alloys—a dislocation pile-up model. *Scripta Metall.* 1979;13:191-194.
- Davidson DL, Lankford J. The effects of aluminum alloy microstructure on fatigue crack growth. *Mater Sci Eng.* 1985;74:189-199.
- Suresh SO, Ritchie RO. Propagation of short fatigue cracks. *Int Met Rev.* 1984;29:445-475.
- Krupp U, Giertler A, Söker M, et al. The behavior of short fatigue cracks during very high cycle (VHCF) fatigue of duplex stainless steel. *Eng Frac Mech.* 2015;145:197-209.
- Ludwig W, Buffière J-Y, Savelli S, Cloetens P. Study of the interaction of a short fatigue crack with grain boundaries in a cast Al alloy using X-ray microtomography. *Acta Mater.* 2003; 51:585-598.
- Birosca S, Buffière J-Y, Karadge M, Preuss M. 3-D observations of short fatigue crack interaction with lamellar and duplex microstructures in a two-phase titanium alloy. *Acta Mater.* 2011;59:1510-1522.
- Schaefer W, Marx M, Vehoff H, Heckl A, Randelzhofer P. A 3-D view on the mechanisms of short fatigue cracks interacting with grain boundaries. *Acta Mater.* 2011;59:1849-1861.
- Tanaka K, Akinawa Y, Nakai Y, Wei RP. Modelling of small fatigue crack growth interacting with grain boundary. *Eng Frac Mech.* 1986;24:803-819.
- Navarro A, De Los Rios ER. Short and long fatigue crack growth: a unified model. *Phil Mag a.* 1988;57:15-36.
- Navarro A, De Los Rios ER. Fatigue crack growth modelling by successive blocking of dislocations. *Proc Royal Soc a: Math Phys Sci.* 1992;437:375-390.
- De Los Rios ER, Xin XJ, Navarro A. Modelling microstructurally sensitive fatigue short crack growth. *Proc Royal Soc a: Math Phys Sci.* 1994;447:111-134.
- Marx M, Schäf W, Vehoff H, Holzapfel C. Interaction of microcracks with selected interfaces: focused ion beam for a systematic crack initiation. *Mater Sci Eng a.* 2006;435:595-601.
- Schäfer F, Weiter L, Marx M, Motz C. Quantifying the grain boundary resistance against slip transfer by experimental combination of geometric and stress approach using stage-I-fatigue cracks. *Phil Mag.* 2016;96:3524-3551.
- Eisenhut L, Schaefer F, Gruenewald P, Weiter L, Marx M, Motz C. Effect of a dislocation pile-up at the neutral axis on trans-crystalline crack growth for micro-bending fatigue. *Int Journal Fatigue.* 2017;94:131-139.
- Motz C, Schöberl T, Pippin R. Mechanical properties of micro-sized copper bending beams machined by the focused ion beam technique. *Acta Mater.* 2005;53:4269-4279.
- Fleck NA, Muller GM, Ashby MF, Hutchinson JW. Strain gradient plasticity: theory and experiment. *Acta Mater.* 1994;42: 475-487.
- Anlas G, Santare MH, Lambros J. Numerical calculation of stress intensity factors in functionally graded materials. *Int J Frac.* 2000;104:131-143.
- Sieböcker D, Knake H, Glatzel U. Temperature dependence of the elastic moduli of the nickel-base superalloy CMSX-4 and its isolated phases. *Mater Sci Eng a.* 2001;298:26-33.
- Gruenewald P, Rauber J, Marx M, Motz C, Schaefer F. Acquiring in situ fatigue crack growth curves by a compliance method for micro bending beams to reveal the interaction of fatigue cracks with grain boundaries. *Proc Struc Integ.* 2019;17:13-20.
- Kiener D, Rester M, Scheriau S, Yang B, Pippin R, Dehm G. Influence of external and internal length scale on the flow stress of copper. *Int Journal Mater Res.* 2007;98:1047-1053.
- Chermahini RG, Shivakumar KN, Newman JC, Blom AF. Three-dimensional aspects of plasticity-induced fatigue crack closure. *Eng Frac Mech.* 1989;34:393-401.
- Wei Y, Hutchinson JW. Steady-state crack growth and work of fracture for solids characterized by strain gradient plasticity. *J Mech Phys Solids.* 1997;45:1253-1273.

How to cite this article: Grünewald P, Rauber J, Marx M, Motz C, Schaefer F. Fatigue crack growth in micro specimens as a tool to measure crack–microstructure interactions. *Fatigue Fract Eng Mater Struct.* 2020;43:3037–3049. <https://doi.org/10.1111/ffe.13354>